AGU PUBLICATIONS

JGR

Journal of Geophysical Research: Space Physics

RESEARCH ARTICLE
10.1002/2014JA020120

Key Points:
- Reconnection sweeps high-energy Na^+-group ions into the cusp from outside
- Low-energy Na^+-group ions were observed upwelling from the cusp
- Protons flowing into the cusp show >40° loss cone in the reflected direction

Correspondence to:
J. M. Raines,
jraines@umich.edu

Citation:
Raines, J. M., D. J. Gershman, J. A. Slavin, T. H. Zurbuchen, H. Korth, B. J. Anderson, and S. C. Solomon (2014), Structure and dynamics of Mercury's magnetospheric cusp: MESSENGER measurements of protons and planetary ions, *J. Geophys. Res. Space Physics*, *119*, 6587–6602, doi:10.1002/2014JA020120.

Received 23 APR 2014
Accepted 28 JUN 2014
Accepted article online 1 JUL 2014
Published online 29 AUG 2014

Structure and dynamics of Mercury's magnetospheric cusp: MESSENGER measurements of protons and planetary ions

Jim M. Raines[1], Daniel J. Gershman[1,2], James A. Slavin[1], Thomas H. Zurbuchen[1], Haje Korth[3], Brian J. Anderson[3], and Sean C. Solomon[4,5]

[1]Department of Atmospheric, Oceanic and Space Sciences, University of Michigan, Ann Arbor, Michigan, USA, [2]Geospace Physics Laboratory, NASA Goddard Space Flight Center, Greenbelt, Maryland, USA, [3]The Johns Hopkins University Applied Physics Laboratory, Laurel, Maryland, USA, [4]Lamont-Doherty Earth Observatory, Columbia University, Palisades, New York, USA, [5]Department of Terrestrial Magnetism, Carnegie Institution of Washington, Washington, District of Columbia, USA

Abstract The MErcury Surface, Space ENvironment, GEochemistry, and Ranging (MESSENGER) spacecraft has observed the northern magnetospheric cusp of Mercury regularly since the probe was inserted into orbit about the innermost planet in March 2011. Observations from the Fast Imaging Plasma Spectrometer (FIPS) made at altitudes < 400 km in the planet's cusp have shown average proton densities (>10 cm^{-3}) that are exceeded only by those observed in the magnetosheath. These high plasma densities are also associated with strong diamagnetic depressions observed by MESSENGER's Magnetometer. Plasma in the cusp may originate from several sources: (1) Direct inflow from the magnetosheath, (2) locally produced planetary photoions and ions sputtered off the surface from solar wind impact and then accelerated upward, and (3) flow of magnetosheath and magnetospheric plasma accelerated from dayside reconnection X-lines. We surveyed 518 cusp passes by MESSENGER, focusing on the spatial distribution, energy spectra, and pitch-angle distributions of protons and Na^+-group ions. Of those, we selected 77 cusp passes during which substantial Na^+-group ion populations were present for a more detailed analysis. We find that Mercury's cusp is a highly dynamic region, both in spatial extent and plasma composition and energies. From the three-dimensional plasma distributions observed by FIPS, protons with mean energies of 1 keV were found flowing down into the cusp (i.e., source (1) above). The distribution of pitch angles of these protons showed a depletion in the direction away from the surface, indicating that ions within 40° of the magnetic field direction are in the loss cone, lost to the surface rather than being reflected by the magnetic field. In contrast, Na^+-group ions show two distinct behaviors depending on their energy. Low-energy (100–300 eV) ions appear to be streaming out of the cusp, showing pitch-angle distributions with a strong component antiparallel to the magnetic field (away from the surface). These ions appear to have been generated in the cusp and accelerated locally (i.e., source (2) above). Higher-energy (≥1 keV) Na^+-group ions in the cusp exhibit much larger perpendicular components in their energy distributions. During active times, as judged by frequent, large-amplitude magnetic field fluctuations, many more Na^+-group ions are measured at latitudes south of the cusp. In several cases, these Na^+-group ions in the dayside magnetosphere are flowing northward toward the cusp. The high mean energy, pitch-angle distributions, and large number of Na^+-group ions on dayside magnetospheric field lines are inconsistent with direct transport into the cusp of sputtered ions from the surface or newly photoionized particles. Furthermore, the highest densities and mean energies often occur together with high-amplitude magnetic fluctuations, attributed to flux transfer events along the magnetopause. These results indicate that high-energy Na^+-group ions in the cusp are likely formed by ionization of escaping neutral Na in the outer dayside magnetosphere and the magnetosheath followed by acceleration and transport into the cusp by reconnection at the subsolar magnetopause (i.e., source 3 above).

1. Introduction

Mercury's northern magnetospheric cusp has been apparent in MErcury Surface, Space ENvironment, GEochemistry, and Ranging (MESSENGER) [*Solomon et al.*, 2007] observations since the beginning of the orbital phase of the mission on 18 March 2011. MESSENGER's Fast Imaging Plasma Spectrometer (FIPS) [*Zurbuchen et al.*, 1998; *Andrews et al.*, 2007] has detected enhancements in solar wind and planetary ion plasma in this region on nearly every orbit [*Zurbuchen et al.*, 2011]. These enhancements span Mercury

latitudes ~30°–80°N and local times 6–14 h. They are found in solar wind protons (H^+) and alpha particles (He^{2+}), as well as planetary ions. Of the planetary ions, Na^+-group ions (a combination of Na^+, Mg^+, and Si^+ ions, ranging in mass per charge between approximately 21 and 30 amu/e [*Zurbuchen et al*., 2011]) are particularly enhanced in the cusp and are on average twice as abundant as solar wind alpha particles [*Raines et al*., 2013]. Depressions in the magnetic field [*Korth et al*., 2011, 2012] have also been observed by the MESSENGER Magnetometer (MAG) [*Anderson et al*., 2007]. These depressions correspond to plasma enhancements, indicating that they are diamagnetic in nature, resulting from the superposition of the main magnetic field and the induced magnetic field of gyrating ions directly opposing the dipole field of Mercury. *Winslow et al*. [2012] used these direct plasma measurements to perform a statistical study of Mercury's cusp region. Their analysis showed that the cusp is a broad, highly variable region located around 56°–84°N magnetic latitude and 7–16 h local time, marking a similar region on Mercury's dayside as the plasma enhancements inferred from direct plasma measurements. This spatial extent is more similar to the V-shaped outer cusp at Earth than the narrow cleft found at lower altitudes [*Smith and Lockwood*, 1996; *Lavraud et al*., 2005]. The high variability in the cusp is attributed to constantly changing solar wind conditions and magnetospheric dynamics. Dayside reconnection [*DiBraccio et al*., 2013] and tail loading and unloading [*Slavin et al*., 2010] likely play substantial roles, but the detailed characteristics of Mercury's cusp are not yet well understood.

At Earth, the cusp is a key dynamical region of the dayside magnetosphere. The historic view of the cusp was based on a fluid picture: The magnetic topology there allows a portion of the magnetosheath flow to be diverted into the cusp [*Spreiter et al*., 1966; *Haerendel et al*., 1978]. The magnetosheath plasma then slows and heats, becoming temporarily trapped and turbulent [*Paschmann et al*., 1976; *Haerendel et al*., 1978]. This view of the Earth's cusp has been largely superseded by one that centers around reconnection. Field lines, newly opened by reconnection at the dayside magnetopause, convect through the cusp, toward the magnetotail [*Dungey*, 1961; *Cowley and Owen*, 1989]. These open field lines serve as entry points for external plasma into the magnetosphere and eventually the ionosphere [*Newell and Meng*, 1988]. Some of this plasma is substantially energized by the reconnection process, which accelerates plasma up to the local Alfvén speed and heats it [*Sonnerup et al*., 1981].

At Mercury, these features of the cusp seem also to be present, though with no collisional atmosphere or an ionosphere to shield it, magnetosheath solar wind can directly impact the surface of the planet [*Kabin et al*., 2000; *Kallio and Janhunen*, 2003; *Kallio et al*., 2008]. An additional dimension in Mercury's cusp is the presence of planetary ions, especially those of the Na^+ group. The role of these ions in cusp dynamics is not known, though with a gyroradius 23 times larger than that of protons of the same temperature, finite gyroradius effects could be prominent in Na^+ transport. Understanding the behavior of Mercury's cusp and the plasma within it, both solar wind and planetary ions will contribute to understanding the planet's overall magnetospheric dynamics.

Simulations have predicted that solar wind impact on the surface will create Na atoms and Na^+ ions in the cusp (Figure 1) [*Lammer et al*., 2003; *Leblanc and Johnson*, 2003, 2010; *Massetti et al*., 2003] over an area that is highly variable [*Kabin et al*., 2000; *Kallio and Janhunen*, 2003; *Kallio et al*., 2008; *Massetti et al*., 2003]. Laboratory experiments have shown that solar wind ions impacting the surface with typical energies of 1–4 keV can cause the release of surface-bound atoms [*Johnson*, 1994]. The effectiveness of this sputtering process depends strongly on the impacting ion flux and energy deposition, as well as many factors that depend on surface composition, such as binding energy and nuclear stopping cross section [*Lammer et al*., 2003]. The sputtered products include neutral atoms (>90%) and ions (<10%), both of which are predicted by simulations to have energies in the 0.01–1 eV range [*Cassidy and Johnson*, 2005]. Impact of solar wind electrons can also release surface-bound atoms in a process called electron-stimulated desorption (ESD). ESD produces neutral atoms and ions in similar proportions to sputtering, but with higher energies, up to 10 eV [*McLain et al*., 2011]. Neutral Na atoms are subject to photoionization, although with an ionization lifetime of ~10,000 s [*Mililo et al*., 2005], most travel away from the cusp on ballistic trajectories before being ionized. Ions are tied to the magnetic field by the Lorentz force so that any velocity component parallel to the magnetic field, together with the mirror force, causes them to stream away from the surface along magnetic field lines, though their perpendicular motion and low energies initially confine them to a small region near their point of ionization. At the altitudes at which MESSENGER passes over the cusp (<1100 km), the high-latitude magnetic field lines extend nearly radially from the planet so that ions

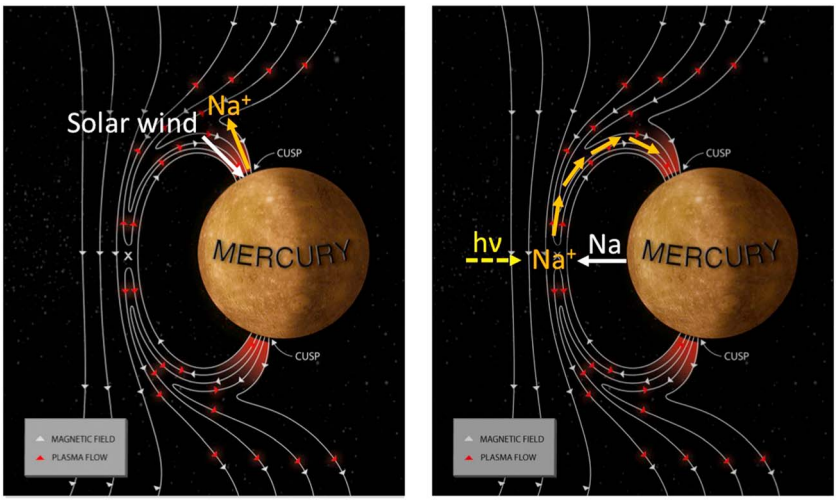

Figure 1. Two possible sources for Na^+ ions in the cusp: (left) Na^+ ions are generated in the cusp, both by solar wind impact and photoionization, and are accelerated by processes there. (right) Neutral Na atoms are ionized near the magnetopause and swept into the cusp.

streaming up from the surface should be detected by FIPS when the sensor's field of view (FOV) is oriented toward the surface. Energization mechanisms local to the cusp are well known at Earth [*Horwitz*, 1984; *Horwitz and Lockwood*, 1985; *Lockwood et al*., 1985]. Several of the same mechanisms have been predicted at Mercury [*Delcourt et al*., 2003, 2012], but none has yet been observed in situ.

Na^+-group ions observed in the cusp may alternatively have their origin outside this region (Figure 1) by means of two possible scenarios. First, neutral Na atoms that have achieved ballistic trajectories across the entire dayside of Mercury could pass through the magnetopause into the magnetosheath and even across the bow shock into interplanetary space, boundaries that do not influence the trajectories of uncharged species. Ions created by photoionization in either of these regions will be picked up into the local convecting flow, experiencing acceleration. The amount of energy gained depends on both the solar wind flow speed and the interplanetary magnetic field (IMF) orientation at the point of pick up [*Moebius et al*., 1985; *Gershman et al*., 2013a, 2014]. Second, Na^+ ions near the magnetopause during a dayside reconnection event could be drawn into the reconnection region and accelerated. This scenario may apply to both Na^+ ions in the magnetosheath and those that are formed in the dayside magnetosphere, as long as they are sufficiently near the magnetopause. That distance could be hundreds of kilometers (or more) and would be determined by the duration of the reconnection and the flow speed of the reconnection inflow jets. Ions swept into the reconnection site or carried with reconnected field lines could be accelerated up to the local Alfvén speed [*Sonnerup et al*., 1981]. Na^+-group ions have been observed in the magnetosheath and outside of the bow shock [*Raines et al*., 2013], consistent with both of these scenarios.

The main purpose of this study is to identify the source of the Na^+-group ions observed in the cusp and to distinguish among the scenarios described above, production and acceleration of planetary ions local to the cusp versus external to it. In the course of examining the characteristics of Na^+-group ions in the cusp, we compare them to those of the protons and, by doing so, are able to elucidate the major properties and behavior of cusp protons as well.

To characterize Na^+-group ions and protons in Mercury's northern hemisphere cusp, we surveyed MESSENGER plasma and magnetic field measurements during the cusp-crossing portions of 518 orbits between September 2011 and May 2012. We took a broad view of the cusp, including both the region of visible diamagnetic depressions in the magnetic field magnitude, $|\mathbf{B}|$, and the extended region of enhanced proton flux. This definition of the cusp arises naturally from the plasma measurements as it encompasses the entire region of enhanced proton flux between two regions that are often mostly empty of plasma, the midlatitude dayside magnetosphere and the northern lobe of the magnetotail. The midlatitude dayside magnetosphere is the region just equatorward of the cusp where magnetic field lines are typically closed. In contrast, the magnetic field lines in the northern lobe of the magnetotail are open. These field lines are

rooted in the planet poleward of the cusp and extend into the magnetotail. On a typical ascending pass, the spacecraft passes from the magnetosheath into the dayside magnetosphere. It then crosses through the cusp and into the northern magnetospheric lobe. For a descending pass, this sequence is reversed.

This paper is organized as follows: We first present time series observations of typical MESSENGER cusp crossings. These cusp passes show a wide range of characteristics of protons and Na^+-group ions in the cusp and the dayside magnetosphere. We then discuss 77 selected cusp crossings with sufficient observed densities of Na^+-group ions ($>3 \times 10^{-3}$ cm^{-3}) and show their average properties, such as ion flow direction and energy distribution relative to the magnetic field. Finally, we use these observations in tandem with the observations of protons in the cusp to infer the likely origin of the observed Na^+-group ions and their major energization processes.

2. Description of Measurements

During the time period of this study, the FIPS sensor measured ions with energy per charge (*E/q*) in the range 0.046–13.3 keV/e (with 6% resolution) and mass per charge (*m/q*) up to 60 amu/e. FIPS has a large instantaneous FOV of 1.4 π sr, though ~0.25 π sr is blocked by the MESSENGER spacecraft and sunshade. For all of the observations analyzed in this study, the FIPS time resolution was about 10 s, the time required for a full *E/q* scan. We focus here on Na^+-group ions. We make extensive use of observed density in our analysis, that is, the density calculated from the measured counts alone, with no attempt to correct for the fraction of the distribution sampled. We have elsewhere reported full ambient plasma densities calculated from FIPS [*Raines et al*., 2011; *Zurbuchen et al*., 2011; *Gershman et al*., 2013b], but those calculations often require assumptions that may not be generally applicable in the cusp and dayside magnetosphere. Additional details of FIPS plasma measurements, the observed density calculation, and ion groups have been given by *Raines et al*. [2013]. MAG operated at its maximum time resolution of 20 vector samples per second for all of the cusp crossings considered here, providing three-dimensional magnetic field data at high cadence.

In this work, we use the observed distributions by angle and energy as the basis for full three-dimensional plasma analysis to provide new insight into cusp plasma distribution and dynamics. We present histograms of ion flow directions, full pitch-angle distributions, and full energy distributions in magnetic coordinates for both protons and Na^+-group ions. These analyses facilitate interpretation of ion motion relative to Mercury and the local magnetic field. They also allow us to infer the behavior of the plasma away from MESSENGER through identification of loss cones and angular asymmetries. We use the highest FIPS angular resolution of 15° when statistics allow, degrading it to 20° for cases in which too few ions were measured.

When transforming FIPS particle observations into a discrete, nondetector-based coordinate system (e.g., those described above), certain bins may be sampled more than others, requiring the computation of a bin-dependent time normalization. To generate this normalization, for each FIPS *E/q* scan, each visible pixel on the FIPS detector was mapped to the appropriate discrete bin in the desired coordinate system and accumulated. This mapping was performed for each individual *E/q* scan to take into account the time evolution of the orientation of FIPS relative to the coordinate system of interest. We neglected any aberration effects due to the spacecraft motion, since they would contribute very little (<2%) to the velocities of the ions. Individual measured events were corrected for efficiency and measurement geometry, accumulated, and then normalized with respect to observation time in each bin to obtain physical units such as flux or phase space density. The product of the solid angle per pixel and efficiency varied by ≤ 35% across the detector, so accumulations across multiple incident angles are not statistically biased by large sensitivity variations, even at low counts.

3. Cusp Observations

We examined each of the 518 cusp passages through a series of analyses as shown in Figures 2–4. In each of these figures, the top panel is the proton energy spectrogram in units of flux (counts s^{-1} cm^{-2} sr^{-1} kV^{-1}). Each vertical column represents one full FIPS energy scan over a period of 10 s. The dimensionless unit steradians are included only by convention, as this flux quantity can be equivalently formulated such that steradians do not naturally appear. The second panel shows the proton pitch-angle distribution (normalized

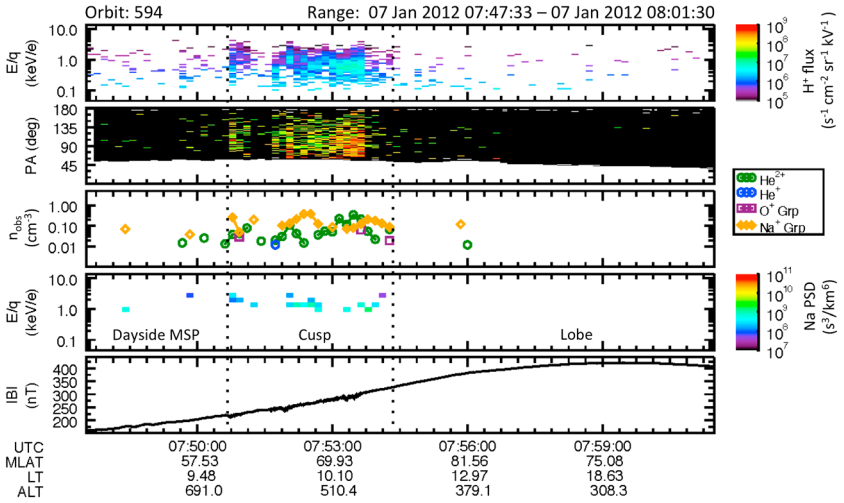

Figure 2. Cusp crossing from orbit 594 (7 January 2012). (first to fifth panels from the top) Shown are the following time series: proton energy spectrogram in units of flux (counts s^{-1} cm^{-2} sr^{-1} kV^{-1}); proton pitch-angle distribution (normalized units); observed number density (cm^{-3}) of alpha particles (He^{2+}, green), He^+ (blue), O^+-group ions (purple), and Na^+-group ions (yellow); Na^+-group ion phase space density (s^3 km^{-6}); and magnetic field intensity (nT). Beneath the bottom panel, several tick marks are labeled with time (UTC), magnetic latitude (MLAT, in °N), local time (LT, in hours), and altitude (ALT, in kilometer). Vertical dotted lines border the cusp region, which lies between the northern magnetospheric lobe and the dayside magnetosphere (MSP).

by maximum flux), the angle between the measured proton velocity vector and the local magnetic field vector. This panel also shows the orientation of the FIPS FOV relative to the magnetic field, and pitch angles outside the FIPS FOV are colored white. We use the proton pitch-angle distribution in this study as a general indicator of plasma behavior in the cusp. With many more counts available, it is much easier to interpret for an individual scan (time step) than the Na^+-group pitch-angle distribution. The third panel shows observed number density in units of cm^{-3}, with each point representing an entire scan. The four species shown on this plot are alpha particles (He^{2+}) and He^+, O^+-group, and Na^+-group ions. The fourth panel shows the energy spectrogram for Na^+-group ions, given in phase space density units of s^3 km^{-6}, to assure that the FIPS sampling in velocity space is properly weighted [*Raines et al.*, 2011]. To make these energies easier to see in the figure, groups of four measured energy bins have been combined, but such a coarser binning has no substantive effect on the interpretation. The fifth panel gives total magnetic field intensity.

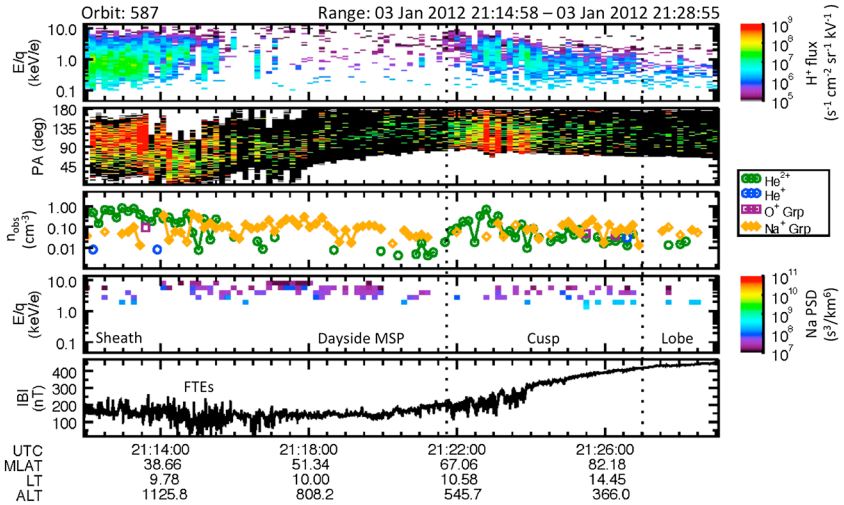

Figure 3. Cusp crossing during an active period (orbit 587, 3 January 2012). See Figure 2 and text for details.

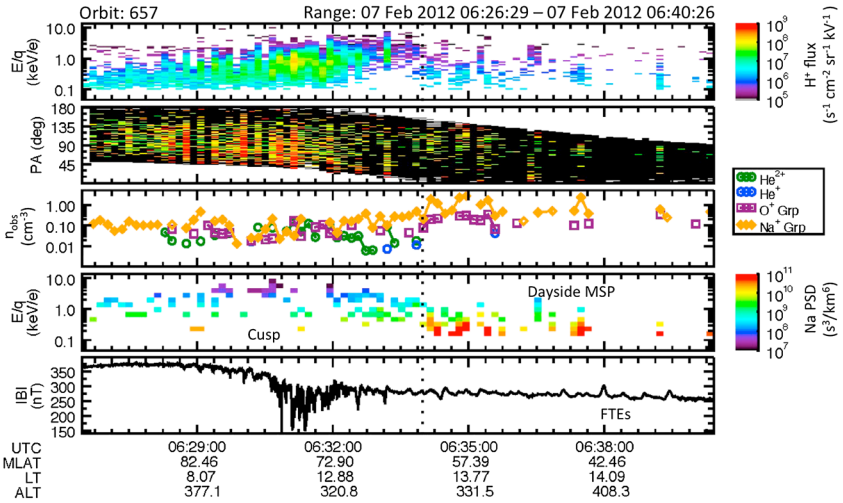

Figure 4. Cusp crossing with low-energy Na^+-group ions in a dayside closed-field region (orbit 657, 7 February 2012). See Figure 2 and text for details.

The first example, shown in Figure 2, shows the cusp crossing for orbit 594 on 7 January 2012. For this event, the cusp crossing has a small spatial extent, lasting just under 3 min or about 620 km along the spacecraft track. The length of the crossing does not necessarily give a complete picture of the cusp size, however, as it depends on the orientation of MESSENGER's orbit and can be affected by cusp dynamics. Most of the Na^+-group ion flux was collocated with that of the alpha particles and protons within the cusp, and only a few scans show Na^+-group ions observed outside the cusp. The energies of measured Na^+-group ions were in the range 0.8–5 keV. The FIPS FOV was downward and toward dawn on this pass so that particles traveling away from the planet were measured. The pitch-angle observations show that ions with pitch angles between ~45° and 180° (away from the surface) can be measured. Most protons had pitch angles in the 45–145° range, with few ions streaming antiparallel to the magnetic field. The record of magnetic field magnitude shows several depressions, which are interpreted as diamagnetic in nature, i.e., the result of increased plasma pressure [*Winslow et al*., 2012; *Korth et al*., 2011, 2012]. The magnetic field magnitude varied smoothly, with few fluctuations larger than ~20 nT in the cusp or dayside region.

Care is required to interpret the relatively narrow range of Na^+-group energies shown in Figure 2. Particle energies appear to cluster around ~1 keV, with no measured phase space density at energies below ~800 eV, misleadingly indicating a cold, fast-flowing plasma. However, as for most plasma analyzers, the FIPS detection threshold decreases with increasing energy along with the volume of phase space measured, i.e., the one-count limit is a lower phase-space density at high energies than at low energies [*Gershman et al*., 2013b]. The very low counts (29) measured in this example result in all but five *E/q* bins having one or two counts in them, indicating that ions with energies below 1 keV were difficult to measure for purely statistical reasons. Therefore, rather than indicating a fast-flowing plasma, this energy signature very likely indicates hot plasma at low density that is at or below the FIPS detection threshold at some energies.

The next cusp example is different and illustrates the contrasting ion populations we found. This case is from seven orbits earlier, orbit 587, on 3 January 2012 (Figure 3). Looking first at the protons, we see considerably higher flux spread over the 5 min cusp crossing, which equates to a cusp dimension of over 1100 km. There is much more variability in the energy spectra, both in distribution and magnitude. Furthermore, an angled feature is evident in the proton energy spectrogram starting around 21:22:00 UTC. This feature appears to be a velocity dispersion signature, which has been shown at Earth to result from the passage of reconnected field lines through the cusp, either from continuous dayside reconnection [*Rosenbauer et al*., 1975] or as part of a flux transfer event (FTE) [*Lockwood and Smith*, 1994]. This signature, which was evident in more than 25 of the cusps surveyed, is caused when higher-energy (faster) particles reach the cusp before the lower-energy (slower) particles. By the time the slower-moving particles reach the cusp, the footpoint of the reconnected field line has moved tailward so that the particles are detected only at higher latitudes. The pitch-angle distributions in this example were mostly centered around 90° and

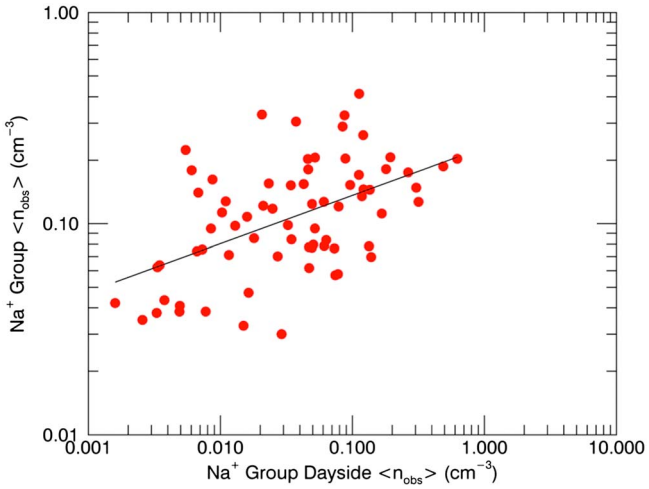

Figure 5. Observed density of Na^+ group ions on the dayside versus that in the cusp on the same orbit. A power law fit to the data (slope = 1.7) is also shown. This figure illustrates that the average observed density of Na^+-group ions on the dayside is weakly correlated with that in the cusp.

especially depleted near 180°, the direction antiparallel to the field and pointing away from the surface. There were several scans of increased flux, all but one of which were centered around 90° pitch angle as well. As with the earlier example, there were substantial alpha particles and Na^+-group ions colocated with the protons. Cusp protons were at higher energies than in the previous example. Na^+-group ion energies seemed to track the protons; they were much higher in this cusp crossing, up to 10 keV. There were also some lower energy (~400 eV) Na^+-group ions present. One substantial difference in this cusp crossing was the presence of substantial Na^+-group ions in the dayside magnetosphere region. These ions appeared near the crossing through the magnetopause, into the dayside magnetosphere, and were measured on nearly every scan up to and through the cusp.

In contrast to the cusp crossing of orbit 594, the magnetic field magnitude in the active cusp was highly variable, showing not only stronger diamagnetic depressions but also rapid (few second duration) fluctuations of up to 100 nT during which the field intensity increased as well as decreased. Some of these transients were likely FTEs that resulted from episodic reconnection [*Slavin et al*., 2012], though detailed analysis of the Magnetometer data is beyond the scope of this work. The measured IMF orientation (not shown) was highly variable just prior to MESSENGER's passage into the magnetosheath.

A third example of a cusp crossing (Figure 4) shows observations for orbit 657 on 7 February 2012. This crossing displays characteristics that are unmatched among the orbits examined in this study. There was a large proton flux, with many bright (higher flux) stripes. The proton flux was spread over nearly 8 min, meaning that the cusp crossing spanned over 1400 km. There were large numbers of planetary ions, both in the cusp and in the dayside region. The diamagnetic depressions in the field strength were particularly large (>100 nT), and enhancements due to FTEs farther outbound (lower in latitude) were also unusually strong. However, this cusp crossing showed another feature: a large population of very low-energy Na^+-group ions in the dayside magnetosphere, just equatorward of the cusp. This feature was rare in the 518 cusps that we surveyed, present in less than 1% of the cases. In the case illustrated in Figure 4, there were also low-energy protons that appeared to be coincident with the very low-energy Na^+-group ions. We discuss the possible source and implications of these low-energy, dayside Na^+-group ions in section 5.

4. Statistical Properties of the Cusp

The examples in Figures 2–4 represent the spectrum of cusp crossings from very weak, small cusps with little proton flux and no Na^+-group ions to large cusps with high proton fluxes and substantial Na^+-group ions in both the cusp and on the dayside. Since the focus of this paper is cusp Na^+, we selected 77 of the total 518 cusps surveyed that had sufficient observed Na^+-group density, at least 3×10^{-3} cm^{-3} Na^+-group ions in the cusp, for further analysis. To give an indication of the range observed in both regions, the average observed density in the cusp is plotted versus average observed density on the entire dayside pass for Na^+-group ions in these 77 events (Figure 5). It is clear from this figure that higher average observed densities on the dayside often occur paired with higher average observed densities within the cusp itself, though this tendency for pairing is not strong (correlation coefficient = 0.31).

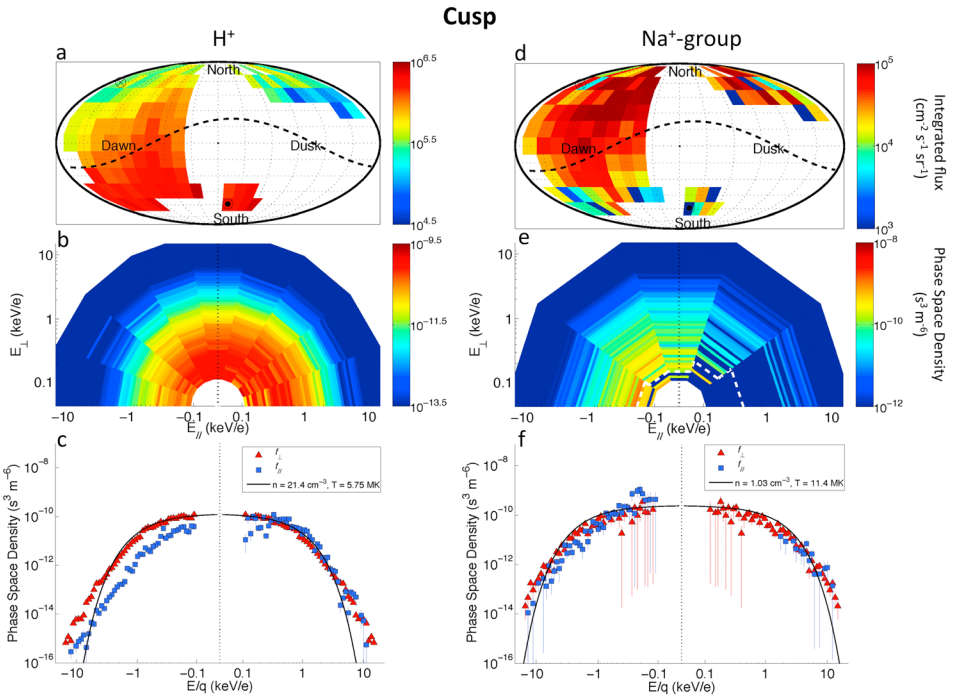

Figure 6. Kinetic properties of protons and Na^+-group ions within the cusp. (a and d) Flow direction histograms for protons and Na^+-group ions. Areas in white denote directions that were not sampled. The average magnetic field direction (pitch angle 0°) is shown by the circle with a dot, whereas the direction opposite to the average magnetic field direction (pitch angle 180°) is shown by the circle with a cross. The direction perpendicular to the average field (pitch angle 90°) is shown as a dashed line. (b and e) Energy-resolved pitch-angle distributions for protons and Na^+-group ions. A dashed white line in the Na^+-group panel indicates the pitch-angle-dependent one-count threshold of FIPS, if it were sampling a stationary, isotropic plasma of the density indicated on the bottom panel. (c and f) Slices of phase-space density versus *E/q* for directions parallel ($f_{||}$, blue squares to the right of the dotted vertical line), antiparallel ($-f_{||}$, blue squares to the left of the dotted vertical line), and perpendicular ($f_{\perp}$, red triangles) to the magnetic field for protons and Na^+-group ions. The black line indicates the prediction for a model distribution (see text). Errors based only on counting statistics are shown as like-colored vertical bars. These figures show protons that are flowing toward the surface, as well as a loss cone >40° in width. Low-energy (100–300 eV) Na^+-group ions appear to be upwelling from the surface, whereas those at energies up to 10 keV have large perpendicular energy components. See text for further details.

For plasma ions, kinetic properties of ion flow direction and energy distribution provide the most fundamental information about their behavior. In Figure 6, we added together three-dimensional FIPS data from the 77 selected cusp crossings to show the average kinetic properties of both protons and Na^+-group ions in the cusp. These accumulations were averaged over a wide range of upstream solar wind conditions and magnetospheric configurations but exhibit average structure with respect to the locally measured magnetic field that are indicative of predominant sources. Figures 6a and 6d show histograms of ion flow direction in units of integrated flux ($cm^{-2}\,s^{-1}\,sr^{-1}$) and divided into 20° angular bins. The coordinate system used is a variant of Mercury solar magnetospheric (MSM) coordinates, but one centered on the FIPS sensor rather than the planetary magnetic dipole. In MSM coordinates, the X_{MSM} axis points from the dipole origin toward the Sun and the Z_{MSM} axis points antiparallel to the planetary dipole, with Y_{MSM} making up a right-handed triad. The view shown is looking from the solar direction, along $-X_{MSM}$. These plots are normalized for viewing time and effects of projection to the MSM coordinate system as described above. The magnetic field direction varied over this accumulation, so it is included only to help orient the reader.

Figures 6b and 6e show energy-resolved pitch-angle distributions in units of phase space density (PSD, $s^3\,m^{-6}$). A pitch-angle resolution of 20° was chosen for protons, whereas 36° resolution was chosen for Na^+-group ions to improve the signal-to-noise ratio. These coadded distributions were assembled from individual scan distributions, computed from the respective scan-averaged magnetic field. The one-count threshold of FIPS (white line in Figure 6e) is pitch-angle dependent because of the varying effective observational times in each bin, as the magnetic field and FIPS FOV vary from scan to scan.

Figures 6c and 6f show slices through the energy-resolved pitch-angle distributions as two-dimensional energy distributions (f) for directions parallel ($f_{||}$), perpendicular ($f_{\perp}$), and antiparallel ($-f_{||}$) to the magnetic field. Moments of these data were taken using the method described by *Gershman et al*. [2013b], for which an isotropic, subsonic Maxwell-Boltzmann distribution with no bulk velocity ($v_0 = 0$) was assumed. These moments, as well as a curve of the modeled distribution, are superimposed over the observed distribution to aid identification and interpretation of departures of the observed distribution from equilibrium.

The angular distribution of cusp protons (Figures 6a–6c) shows that these particles are flowing in a wide range of directions, though some are clearly flowing southward, toward the planet (Figure 6a). This spread in ion flow direction is consistent with hot plasma of low sonic Mach number. The distribution of phase-space density (Figure 6b) is relatively isotropic for directions parallel through perpendicular to the local magnetic field, indicative of plasma with nearly equivalent parallel and perpendicular temperatures. The distribution seems to be offset in the parallel direction, toward the surface. There is also a clear depletion in the antiparallel direction, away from the surface. These features are also apparent in the energy distributions. In Figure 6c, to the right of the dotted line, $f_{||}$ is slightly larger, especially around 1 keV, than $f_{\perp}$. To the left of the dotted line, the opposite is true: $-f_{||}$ is noticeably lower than $f_{\perp}$. We interpret these results as indicating that hot protons are flowing into the cusp from the magnetosheath, as indicated in their energy distributions by large perpendicular components and a parallel (i.e., planetward) enhancement. Ions with a dominant perpendicular component to their energy mirror in the magnetic field and move radially outward from the cusp. Those that are more closely aligned with the field, however, are within the loss cone and impact the planet below the cusp. The proton energy distribution (Figure 6b) shows this pattern in the marked dropoff of particles in the 140–160° and 160–180° bins, indicating that the cutoff pitch angle is ≤ 140°, creating a loss cone of ≥ 40° in width for this subset of cusp passes.

The distribution of Na^+-group ions (Figures 6d–6f) differs substantially from that of the protons. Figure 6d shows that most ions are traveling in directions that are perpendicular to (dawn) or away from the surface (north). This pattern is consistent with the energy-resolved pitch-angle distribution (Figure 6e), which indicates that ions are traveling either in the antiparallel direction (away from the surface) or have mostly perpendicular energy components. The $-f_{||}$ slice through the energy-resolved pitch-angle distribution (Figure 6f) shows that low-energy (≤300 eV) ions are streaming out of the cusp (blue squares), antiparallel to the magnetic field and are thus substantially enhanced over the $f_{\perp}$ slice. At higher energies, 300 eV to 6 keV, the distribution nearly follows the modeled isotropic Maxwell-Boltzmann distribution, showing just a slight depletion of $-f_{||}$ relative to $f_{\perp}$. On the parallel side ($f_{||}$), fewer particles are measured, but where present, $f_{||} \sim f_{\perp}$. This distribution ($f_{||}$) appears similar in shape to the left side ($-f_{||}$) relative to the modeled Maxwellian.

The observations in the dayside magnetosphere (south of the cusp latitude) necessitate a more restricted analysis. Figure 7 shows histograms of the flow direction for protons and Na^+-group ions on orbit 587 in the cusp and in the dayside magnetosphere. In the cusp, both protons and Na^+-group ions are traveling in a broad range of directions, though mostly in directions around the 90° pitch angle line. This situation is much like that observed in the statistical distribution shown in accumulations (Figure 6). In contrast, however, in the dayside magnetosphere (Figure 7d) the Na^+-group ions are moving coherently north, in what looks to be a broad beam. Furthermore, this beam appears to be largely perpendicular to the magnetic field. This behavior is much less clear in the histogram of dayside proton flow directions, possibly because of low proton counts there. Some of the protons are moving north, like the Na^+-group ions, but there are protons traveling in directions all around the dayside. The same information is presented for orbit 413 in Figure 8. As described for orbit 587, the direction of travel for protons in the cusp (Figure 8a) is rather broadly distributed around the 90° pitch-angle line. In contrast, however, the majority of protons in the dayside magnetosphere (Figure 8b) are much more focused, apparently forming a beam in the direction of midlatitudes in the northern hemisphere. The Na^+-group ions on the dayside are traveling in much the same direction but not as clearly in a beam distribution as the protons.

The presence of beam distributions has two important implications for the interpretation of our data. First, the plasma appears to be moving largely perpendicular to the magnetic field. This behavior could indicate that the plasma is on moving field lines or has been recently picked up. Second, this motion causes the parallel and perpendicular energy distributions to no longer reflect only the thermal properties of the distribution. We therefore restricted our analysis of these distributions to ion flow direction

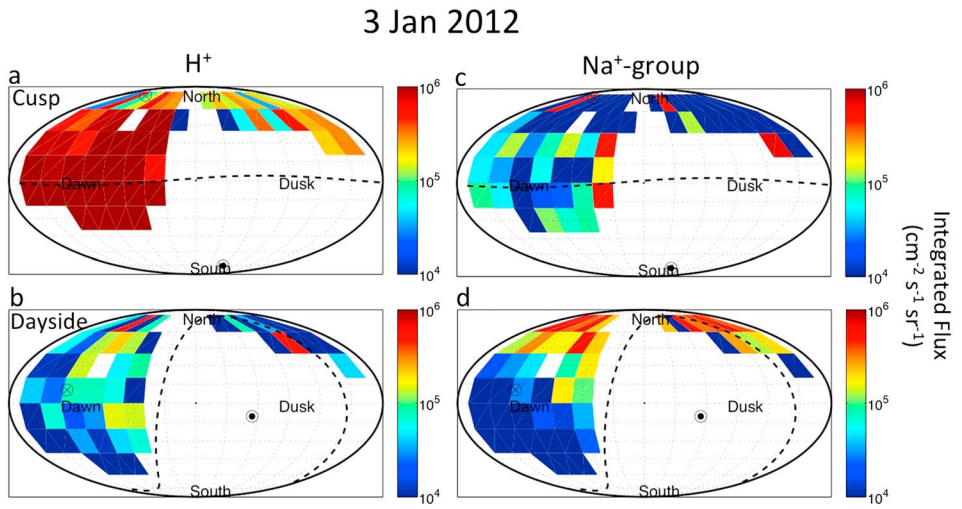

Figure 7. Ion flow direction histograms for protons and Na^+-group ions on orbit 587 (3 January 2012) separated into (a and c) cusp and (b and d) dayside magnetosphere regions. The dayside magnetosphere region shows northward flow, as would be expected from dayside reconnection.

histograms. We examined these histograms for 11 of the 77 cusps to assess the generality of the beam distributions. We found dayside regions on two other orbits that clearly showed beams: 29 September 2013, 22:05:00–22:11:00 UTC (orbit 393) and 13 October 2011, 15:19:45–15:36:30 UTC (orbit 421). Dayside magnetosphere regions from other orbits of the 11 examined showed some evidence of beaming, e.g., orbit 657 from Figure 4 above, but the signature was not as clear. The character of the beam signature will depend on the relative orientation of the spacecraft passage through the cusp, the FIPS FOV orientation, and the direction of plasma motion. Because of this variability, summed statistical distributions, such as that used for Figure 6 in the cusp, are unlikely to reflect the properties of individual cases. This fact, along with the qualitative nature of these directional histograms, makes more general identification of the beams challenging and requires more extensive data coverage that is beyond the scope of this work. Nonetheless, the presence of beam distributions, which these events establish, is an important point to which we return in section 5.

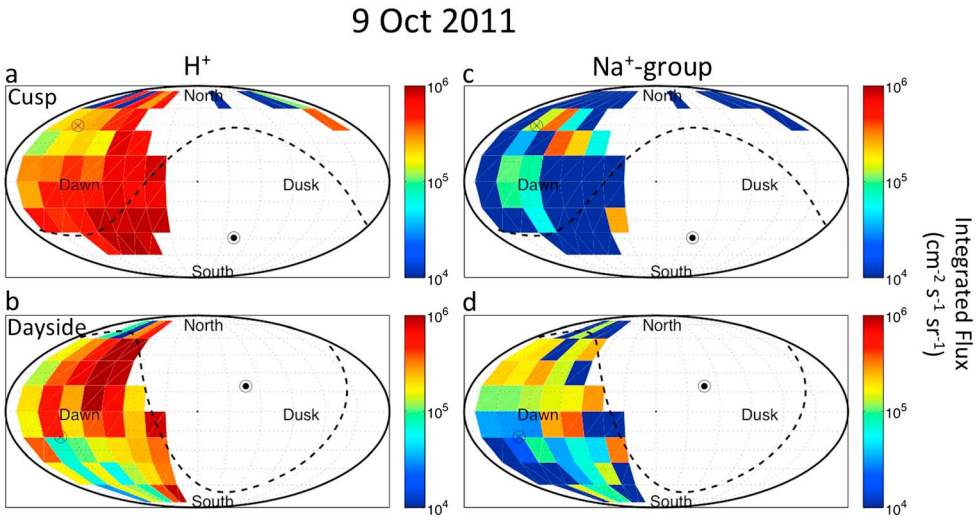

Figure 8. Ion flow direction histograms for protons and Na^+-group ions on orbit 413 (9 October 2011) separated into (a and c) cusp and (b and d) dayside regions. A northward flow of protons is clearly apparent in the dayside magnetosphere (Figure 8b).

5. Discussion

5.1. Sources of High-Energy (≥1 keV) Na^+-Group Ions

We described three hypotheses for the origin of the observed Na^+-group ions: (1) Na^+-group ions are ejected by interaction of the solar wind with Mercury's surface at the cusp via solar wind sputtering and ESD; (2) neutral Na atoms are photoionized upstream of the magnetopause and subsequently swept back into the cusp by the plasma flow; or (3) neutral Na atoms are photoionized in the vicinity of the magnetopause and swept into the cusp as part of dayside reconnection. It is immediately clear that most of the ions observed by FIPS in the cusp are not simply ejected from the surface or photoionized from exospheric neutrals there. The observed ions have substantially higher energies (2.7 keV on average) than has been estimated for sputtering (~1 eV) [*Cassidy and Johnson*, 2005] or ESD, which would result in Na^+ energies < 10 eV [*McLain et al*., 2011]. It may be possible that ions that have been either photoionized from the exosphere or ejected directly from the surface and later accelerated prior to measurement by FIPS could account for their high average energies. To evaluate this possibility, we examine several cusp-localized acceleration mechanisms that have been reported at Earth.

One acceleration mechanism with a cusp-localized component reported at Earth is known as the "cleft ion fountain" [*Horwitz*, 1984; *Horwitz and Lockwood*, 1985; *Lockwood et al*., 1985]. Test particle simulations by *Horwitz* [1984] showed that ions released in the northern cusp with the right energy (0.3–0.5 eV) could follow a curved trajectory back into the magnetotail, staying within the magnetosphere. This acceleration is quite sensitive to the initial energy of the ions and the cross-polar-cap electric field. Increasing the field and lowering the energy of the ions increases trapping. *Horwitz and Lockwood* [1985] further showed particular examples whereby cusp ions could be energized by a factor of 10 in many cases due to a combination of $\mathbf{E} \times \mathbf{B}$ drift (where $\mathbf{E}$ is the local electric field) and magnetic field gradients along the field lines. *Delcourt et al*. [2012] applied a very similar simulation technique to Mercury, expanded into three dimensions and explicitly including the full equations of motion, to study centrifugal acceleration of ions traveling from the cusp into the magnetotail. They showed that largely due to the curvature of $\mathbf{E} \times \mathbf{B}$ drift paths, ions can be accelerated from energies of < 0.1 eV up to several hundred eV as they traverse the magnetospheric tail lobes. This effect is more pronounced at Mercury than at Earth because of the large fractional volume of Mercury's magnetosphere occupied by the planet. Greater magnetic field curvature and more rapid convection result, leading to stronger centrifugal acceleration.

However, this mechanism is very unlikely to account for the observed ions with ≥ 1 keV energies within the cusp. The ions in the simulation by *Delcourt et al*. [2012] were accelerated to keV energies, but the acceleration took place over a much longer path length than the size of the cusp. Acceleration achieved within the cusp by this mechanism should be a fraction of the total reported, yielding particle energies lower than observed. Furthermore, acceleration in the cusp should produce ions that are streaming along field lines out of the cusp. The superposed pitch-angle distribution for Na^+-group ions in the cusp (Figure 6e) does not show field-aligned streaming but rather a substantial population spanning 90° pitch angles above 300 eV. Finally, for acceleration local to the cusp, we would expect a reverse velocity dispersion signature in the Na^+-group energies: Ion energy should increase with latitude within the cusp. This mechanism accelerates ions antisunward, so ions measured at higher latitudes should have been accelerated more by the time they are measured than those measured at lower latitudes. This pattern was not observed in our inspection of the 77 selected cusps. It is clear that this acceleration mechanism is not capable of accelerating cusp ions from < 10 eV to the observed ≥ 1 keV energies within the cusp region.

Another possible acceleration mechanism for planetary ions in the cusp is wave-particle interaction. At Earth, for example, *Ashour-Abdalla et al*. [1981] documented examples of heating of cusp protons and oxygen ions by ion-cyclotron waves. In that study, the initial free energy source was shown to be electrons flowing down into the cusp from the magnetosheath. This mechanism was shown to account for an energy gain by factors of 2 and 6 over the initial value for H^+ and O^+, respectively. Essentially all of this energy gain was in the perpendicular direction, with very little parallel acceleration. This energy gain is insufficient to explain the observed high-energy Na^+-group ions in Mercury's cusp, however. Simulations by *Retterer et al*. [1983] predicted that lower hybrid waves could energize ions to ≥ 1 keV, starting with an initial energy of 1 eV, by forming ion conic distributions. In this scenario, ions are heated by lower hybrid waves coupled to the incoming electron distributions, with a final energy that depends in part on the size of the acceleration

region. Similar heating of cusp O^+ ions by lower hybrid waves excited by ring distributions has also been observed [*Roth and Hudson*, 1985]. These mechanisms may also be in action at Mercury, but it is unlikely that the smaller spatial scale and residence times associated with Mercury's cusp would allow energization to the same extent as at Earth. If present, the temperature anisotropies created could potentially excite other wave modes that could provide additional acceleration. In any event, the instrumentation on MESSENGER is insufficient to confirm the presence of the required lower hybrid waves.

Ions energized elsewhere in Mercury's magnetosphere and environment and then swept into the cusp would have very different properties from those generated locally in the cusp. If the ions were swept in from the solar wind, they would first have to be picked up into the solar wind flow. When the solar wind is diverted around the magnetosphere, it slows down, to the point that it is nearly stagnant at the subsolar point and is nearly at its original speed, v_{sw}, at ~90° from the subsolar point [*Spreiter et al*., 1966]. The fraction of the flow speed gained during ion pickup also depends on the orientation of upstream solar wind or draped magnetosheath IMF [*Slavin et al*., 2008]. A larger magnetic field component perpendicular to the flow direction leads to more pickup energization. The IMF at Mercury tends to be quasi-radial, resulting in average ion speeds up to ~1 v_{sw} [*Gershman et al*., 2014]. Ions created outside of the bow shock will be further heated as they pass through the shock. The magnetic field in the magnetosheath tends to drape around the magnetopause almost independently of the upstream IMF direction, with expected flows also tangent to the magnetopause boundary [*Gershman et al*., 2013b]. This configuration should also result in ions created in the magnetosheath energized up to ~1 v_{sw}. Given a nominal 440 km/s solar wind speed, the flow speed in the magnetosheath at the location of the cusp (~65°N) should be ~220 km/s (~0.5 v_{sw}). For a Na^+ ion, this speed corresponds to an energy of 6 keV, which is in the range of ion energies observed. The corresponding bulk speed could be converted to thermal speed by the increasing magnetic field in the cusp, as the plasma particles are subject to an increasing magnetic mirror force converting their parallel energy to perpendicular energy. Furthermore, the high levels of magnetic fluctuations in the cusp likely indicate substantial plasma wave power there. These waves would tend first to scatter ions into a shell in velocity space, spreading their energy across many directions with respect to the magnetic field. After a short time, these waves would serve to drive particle distribution functions to equilibrium Maxwell-Boltzmann distributions. As was discussed above, the energy distribution in the cusp (Figures 6e and 6f) shows substantial perpendicular energy, consistent with this scenario. However, particles with sufficient parallel energy, i.e., within the loss cone in the planetward (parallel) direction, would be lost to the surface. These lost ions would not mirror in the increasing cusp field, leading to a depletion of particles in the antiparallel direction, similar to that observed for the protons (Figure 6b). This pattern is not observed for the Na^+-group ions, however (Figure 6e). Instead, the 144–180° energy bin shows that substantial numbers of particles are moving antiparallel to the field. Except for an enhancement of ions in the 100–300 eV range (discussed below), the PSD in this bin appears quite similar to that in the adjacent angular bin. It therefore seems unlikely that the majority of these ≥ 1 keV Na^+-group ions are swept into the cusp from solar wind pickup and subsequent flow into the cusp from the magnetosheath.

Alternatively, ions could be swept into the cusp by reconnection. At hundreds of kilometers, the gyroradii of Na^+-group ions with ≥ 1 keV energies are too large for the ions to be accelerated directly by the reconnection process, which occurs at most on the scale of proton gyroradii (~20 times smaller). However, tied to the field lines, they would still experience substantial acceleration as those field lines reconnect and are swept northward toward the cusp. These field lines would move at speeds up to the local Alfvén speed (v_A). For an average solar wind density of 50 cm^{-3} at 0.3 AU, the density at the subsolar stagnation point could be up to 200 cm^{-3} [*Gershman et al*., 2013b]. For a magnetic field strength of 133 nT at the subsolar point [G. A. DiBraccio, private communication, 2013], the Alfvén speed would be 265 km/s. This speed corresponds to a particle energy of 8.4 keV for Na^+, in the same range as that observed. This motion would lead to Na^+-group ions with large perpendicular energies, consistent with observations (Figures 6d and 6e). Additionally, ion flow direction histograms are consistent with northward-traveling ions for several representative cases (Figures 7 and 8), as expected for reconnected field lines. Finally, plasma inflow to a dayside reconnection region may draw in ions from a substantial fraction of the dayside. This inflow to the reconnection site is typically at a speed of about 0.1–0.2 v_A [*Sonnerup*, 1974] or ~26–52 km/s from our estimate above. For a reconnection event lasting 10–20 s and a Dungey cycle duration of ~2 min [*Slavin et al*., 2008], ions would be swept in from up to 1000 km from the magnetopause. This process may be evident

in Figures 4 and 5: A steady stream of protons, alpha particles, and planetary ions was measured by FIPS as MESSENGER traversed the dayside region, a feature that occurred clearly in over half of the 77 cusp crossings examined.

Given the arguments above, we may make two conclusions about Na^+-group ions with energy ≥ 1 keV observed by FIPS: (1) High-energy Na^+-group ions observed in the cusp have been transported from elsewhere, rather than accelerated locally in the cusp, and (2) the evidence of cuspward plasma flow and the general trend for the highest observed Na^+-group energies to occur with high magnetic field fluctuations indicates that dayside reconnection plays an important role in their energization.

5.2. Sources of Low-Energy (≤300 eV) Na^+-Group Ions

Although less prevalent than the higher-energy populations, < 1 keV Na^+-group ions are observed in the cusp and in the dayside magnetosphere. The most abundant of these have energies in the range 100–300 eV, so we focus on those here. Exospheric neutrals have been observed with a wide range of temperatures by the MESSENGER Ultraviolet and Visible Spectrometer on the Mercury Atmospheric and Surface Composition Spectrometer instrument [*McClintock and Lankton*, 2007]: 1000–5000 K for Na, 20,000 K for Mg, and up to 50,000 K for Ca [*Vervack et al*., 2010; *Burger et al*., 2012]. These temperatures correspond to Na energies of ~0.22 eV or up to ~ 2 eV for three standard deviations from the mean. As discussed above, the upper energy limit for neutrals released from the surface estimated from ESD is 100,000 K (10 eV) [*McLain et al*., 2011]. Neutrals that are photoionized in the dayside magnetosphere may become trapped on closed dayside field lines at basically their same energy, since photoionization will not markedly change the kinetic energy of the particle. To escape Mercury's gravity, an atom must have a speed of 4.3 km/s [*Hunten et al*., 1988], corresponding to 2.2 eV for a Na^+ ion. These ion energies are too low by a factor of 10 to account for ions observed in the 100–300 eV energy range.

Nonetheless, the energy distribution of low-energy Na^+-group ions (Figure 6f) clearly shows a substantial enhancement in the 100–300 eV energy range, which we interpret as an upwelling component. This observation is a strong indication that acceleration in the cusp at Mercury produces ions in that energy range from the very low-energy ions (<10 eV) expected there. These higher-energy ions could have been accelerated by the processes described in section 5.1. In particular, it has been shown that Na^+ ions released from the cusp are accelerated by the centrifugal force created by the curvature of their $\mathbf{E} \times \mathbf{B}$ drift paths [*Delcourt et al*., 2003, 2012; *Sarantos et al*., 2009], with more acceleration for higher cross-polar-cap potentials. Though *Delcourt et al*. [2012] showed energization up to only 50 eV within the cusp, their study used a lower cross-polar-cap potential (10 kV maximum) than has since been found at Mercury. *DiBraccio et al*. [2013] found an average cross-polar-cap potential of 30 kV, with excursions of up to 80 kV. The resulting increased acceleration could have brought very low-energy ions into the observed 100–300 eV range. Higher-energy Na^+-group ions present in the antiparallel (154–180°) pitch-angle bin (Figure 6e) are not likely to be an upwelling component because of the energy arguments discussed in the previous section. Furthermore, their distribution in energy appears to be much more isotropic in pitch angle (Figure 6e) and like a Maxwell-Boltzmann distribution (Figure 6f). These particles have likely been scattered into this pitch-angle range by processes in the cusp. The fact that the proton loss cone is not empty (Figure 6b) is further evidence of these processes at work.

An additional source for the observed 100–300 eV ions may be circulation inward from the magnetotail. It is well known that plasma in Earth's magnetotail flows back toward the planet and around the equatorial region to the dayside as a result of Dungey-cycle convection [*Dungey*, 1961]. Evidence of this flow pattern at Mercury has been observed in the form of dipolarization signatures [*Sundberg et al*., 2012], which indicate planetward plasma flow in the magnetotail resulting from reconnection in the cross-tail current sheet. In order for planetary ions to make it back around to the dayside, their gyroradii must fit inside the dayside magnetosphere. As their gyroradius increases, the channel through which they can pass without gyrating into the planet or across the magnetopause and being lost effectively narrows. *Winslow et al*. [2013] found a mean magnetopause standoff distance of 1.45 R_M from the planet center (where R_M is Mercury's radius), or 980 km altitude. The dayside portion of the magnetopause is approximately hemispherical [*Shue et al*., 1997; *Slavin et al*., 2010], so this measurement sets the approximate size of the dayside magnetosphere.

Here we use the Alexeev magnetic field model [*Alexeev et al*., 2008, 2010] to calculate typical ion gyroradii over a range of energies, from 100 eV to 8 keV, in the dayside magnetosphere 1.2 R_M from the planet center

Table 1. Sample Clearance Distances for a Gyrating Na^+ Ion Calculated From Modeled Magnetic Field at Locations Specified in the Equatorial Dayside Magnetosphere

Location (MSM)		Energy	Field	Gyroradius		Distance (R_M)	
X (R_M)	Y (R_M)	E (keV)	B (nT)	(km)	(R_M)	MP	surface
1.20	0.00	0.2	177	55	0.023	0.207	0.177
1.20	0.00	2	177	175	0.072	0.158	0.128
1.20	0.00	4	177	247	0.101	0.129	0.099
1.20	0.00	8	177	350	0.143	0.087	0.057
0.00	1.20	0.2	130	75	0.031	0.199	0.169
0.00	1.20	2	130	238	0.098	0.132	0.102
0.00	1.20	4	130	337	0.138	0.092	0.062
0.00	1.20	8	130	476	0.195	0.035	0.005

(490 km altitude). We assume that all of the measured energy was in the perpendicular direction, yielding the largest equatorial gyroradius and thus a bounding case. The results are shown in Table 1. These simple calculations show that ions of these energies could fit through the equatorial dayside magnetosphere, between the magnetopause (MP) and the surface. It is also apparent that lower-energy ions have much more clearance in the dayside magnetosphere, which in turn allows a greater range of trajectories to pass through. Transport through this region may act like an energy filter, preferentially allowing more low-energy (100–300 eV) ions to pass than high-energy (1–10 keV) ions. Of course, the solar wind conditions would also play a role. When the solar wind dynamic pressure increases, due to increases in solar wind density, velocity, or both, the magnetopause will be compressed and move closer to the planet. Conversely, dynamic pressure decreases will increase the size of the space. We have previously reported that planetary ions are observed in Mercury's magnetotail [*Zurbuchen et al.*, 2011]. In the few cases examined, the ions observed had energies $>$ 1 keV, but no attempt was made to search for low-energy ions in the magnetotail.

5.3. Protons in the Cusp

As expected from modeling studies at Mercury and previous studies for Earth, protons in the cusp are found to be flowing downward toward the surface (Figure 6b). Given energies around 1 keV, these protons likely have traveled into the cusp from the magnetosheath or from dayside reconnection. However, if they participated in reconnection, the protons very likely experienced acceleration parallel to the magnetic field in reconnection jets since their gyroradii are not large relative to typical FTE dimensions [e.g., *Slavin et al.*, 2012; *DiBraccio et al.*, 2013]. These protons are also quite hot, as indicated by their substantial perpendicular energy and large estimated temperature (5.75 MK). The presence of a loss cone, of width $\geq 40°$, is a strong indication that a portion of these protons are precipitating onto the surface. These observations are the best indication thus far that predicted space weathering processes in the cusp are actually occurring.

6. Conclusions

We studied MESSENGER cusp crossings for 518 orbits from September 2011 through May 2012. We found that Na^+-group ions are routinely observed in the cusp region with energies in the 0.8–4 keV range (2.7 keV average, 13 keV maximum) and observed densities of 0.01–2 cm^{-3}. There is substantial variability in the cusp for all species. High-energy ($\geq$ 1 keV) Na^+-group ions are observed with large perpendicular energies in the cusp. We also found high-energy Na^+-group ions traveling northward in the dayside magnetosphere (south of the cusp). Their occurrence frequency is highest in conjunction with strong diamagnetic decreases and magnetic field fluctuations, due in part to FTEs. We therefore conclude that observations of these high-energy Na^+-group ions strongly favor the explanation that they are ionized in the neighborhood of the magnetopause and then swept into the cusp by reconnection.

Low-energy (100–300 eV) Na^+-group ions are also observed, both in the cusp and at times in the dayside magnetosphere. Pitch-angle distributions in the cusp show that these ions are upwelling from the surface. We therefore conclude that a portion of the low-energy Na^+-group ions are generated in the cusp and accelerated there as well. We infer that a portion of these ions may also be brought into the dayside

magnetosphere through Dungey circulation from the magnetotail or by ion drift. Finally, we find that protons appear to be flowing down into the cusp from the magnetosheath, as predicted by simulations and observed at Earth. A portion of these protons appears to be lost to surface precipitation, allowing us to put a lower bound of 40° on the northern cusp loss cone for these ions.

Acknowledgments

The MESSENGER project is supported by the NASA Discovery Program under contracts NAS5-97271 to The Johns Hopkins University Applied Physics Laboratory and NASW-00002 to the Carnegie Institution of Washington. J.M.R. thanks D. Schriver and T. A. Cassidy for discussions helpful to this work. Data used in this study are available from the Planetary Data System.

Yuming Wang thanks Brian Walsh and an anonymous reviewer for their assistance in evaluating this paper.

References

Alexeev, I. I., E. S. Belenkaya, S. Y. Bobrovnikov, J. A. Slavin, and M. Sarantos (2008), Paraboloid model of Mercury's magnetosphere, *J. Geophys. Res.*, *113*, A12210, doi:10.1029/2008JA013368.

Alexeev, I. I., et al. (2010), Mercury's magnetospheric magnetic field after the first two MESSENGER flybys, *Icarus*, *209*, 23–39, doi:10.1016/j.icarus.2010.01.024.

Anderson, B. J., M. H. Acuña, D. A. Lohr, J. Scheifele, A. Raval, H. Korth, and J. A. Slavin (2007), The Magnetometer instrument on MESSENGER, *Space Sci. Rev.*, *131*, 417–450, doi:10.1007/s11214-007-9246-7.

Andrews, G. B., et al. (2007), The energetic particle and plasma spectrometer instrument on the MESSENGER spacecraft, *Space Sci. Rev.*, *131*, 523–556, doi:10.1007/s11214-007-9272-5.

Ashour-Abdalla, M., H. Okuda, and C. Z. Cheng (1981), Acceleration of heavy ions on auroral field lines, *Geophys. Res. Lett.*, *8*, 795–798, doi:10.1029/GL008i007p00795.

Burger, M. H., R. M. Killen, W. E. McClintock, R. J. Vervack Jr., A. W. Merkel, A. L. Sprague, and M. Sarantos (2012), Modeling MESSENGER observations of calcium in Mercury's exosphere, *J. Geophys. Res.*, *117*, E00L11, doi:10.1029/2012JE004158.

Cassidy, T. A., and R. E. Johnson (2005), Monte Carlo model of sputtering and other ejection processes within a regolith, *Icarus*, *176*, 499–507, doi:10.1016/j.icarus.2005.02.013.

Cowley, S. W. H., and C. J. Owen (1989), A simple illustrative model of open flux tube motion over the dayside magnetopause, *Planet. Space Sci.*, *37*, 1461–1475, doi:10.1016/0032-0633(89)90116-5.

Delcourt, D. C., S. Grimald, F. Leblanc, J. J. Berthelier, A. Millilo, A. Mura, S. Orsini, and T. E. Moore (2003), A quantitative model of the planetary Na^+ contribution to Mercury's magnetosphere, *Ann. Geophys.*, *21*, 1723–1736, doi:10.5194/angeo-21-1723-2003.

Delcourt, D. C., K. Seki, N. Terada, and T. E. Moore (2012), Centrifugally stimulated exospheric ion escape at Mercury, *Geophys. Res. Lett.*, *39*, L22105, doi:10.1029/2012GL054085.

DiBraccio, G. A., J. A. Slavin, S. A. Boardsen, B. J. Anderson, H. Korth, T. H. Zurbuchen, J. M. Raines, D. N. Baker, R. L. McNutt Jr., and S. C. Solomon (2013), MESSENGER observations of magnetopause structure and dynamics at Mercury, *J. Geophys. Res. Space Physics*, *118*, 997–1008, doi:10.1002/jgra.50123.

Dungey, J. W. (1961), Interplanetary magnetic field and auroral zones, *Phys. Rev. Lett.*, *6*, 47–48, doi:10.1103/PhysRevLett.6.47.

Gershman, D. J., G. Gloeckler, J. A. Gilbert, J. M. Raines, L. A. Fisk, S. C. Solomon, E. C. Stone, and T. H. Zurbuchen (2013a), Observations of interstellar helium pickup ions in the inner heliosphere, *J. Geophys. Res. Space Physics*, *118*, 1389–1402, doi:10.1002/jgra.50227.

Gershman, D. J., J. A. Slavin, J. M. Raines, T. H. Zurbuchen, B. J. Anderson, H. Korth, D. N. Baker, and S. C. Solomon (2013b), Magnetic flux pile-up and plasma depletion layers in Mercury's subsolar magnetosheath, *J. Geophys. Res. Space Physics*, *118*, 7181–7199, doi:10.1002/2013JA019244.

Gershman, D. J., L. A. Fisk, G. Gloeckler, J. M. Raines, J. A. Slavin, T. H. Zurbuchen, and S. C. Solomon (2014), The velocity distribution of pickup He^+ measured at 0.3 AU by MESSENGER, *Astrophys. J.*, *788*, 124, doi:10.1088/0004-637X/788/2/124.

Haerendel, G., G. Paschmann, N. Sckopke, and H. Rosenbauer (1978), The frontside boundary layer of the magnetosphere and the problem of reconnection, *J. Geophys. Res.*, *83*, 3195–3216, doi:10.1029/JA083iA07p03195.

Horwitz, J. L. (1984), Features of ion trajectories in the polar magnetosphere, *Geophys. Res. Lett.*, *11*, 1111–1114, doi:10.1029/GL011i011p01111.

Horwitz, J. L., and M. Lockwood (1985), The cleft ion fountain: A two-dimensional kinetic model, *J. Geophys. Res.*, *90*, 9749–9762, doi:10.1029/JA090iA10p09749.

Hunten, D. M., T. H. Morgan, and D. E. Shemansky (1988), The Mercury atmosphere, in *Mercury*, edited by F. Vilas, C. R. Chapman, and M. S. Matthews, pp. 562–612, Univ. Arizona Press, Tucson, Ariz.

Johnson, R. E. (1994), Plasma-induced sputtering of an atmosphere, *Space Sci. Rev.*, *69*, 215–253, doi:10.1007/BF02101697.

Kabin, K., T. I. Gombosi, D. L. DeZeeuw, and K. G. Powell (2000), Interaction of Mercury with the solar wind, *Icarus*, *143*, 397–406, doi:10.1006/icar.1999.6252.

Kallio, E., and P. Janhunen (2003), Solar wind and magnetospheric ion impact on Mercury's surface, *Geophys. Res. Lett.*, *30*(17), 1877, doi:10.1029/2003GL017842.

Kallio, E., et al. (2008), On the impact of multiply charged heavy solar wind ions on the surface of Mercury, the Moon and Ceres, *Planet. Space Sci.*, *56*, 1506–1516, doi:10.1016/j.pss.2008.07.018.

Korth, H., B. J. Anderson, J. M. Raines, J. A. Slavin, T. H. Zurbuchen, C. L. Johnson, M. E. Purucker, R. M. Winslow, S. C. Solomon, and R. L. McNutt Jr. (2011), Plasma pressure in Mercury's equatorial magnetosphere derived from MESSENGER Magnetometer observations, *Geophys. Res. Lett.*, *38*, L22201, doi:10.1029/2011GL049451.

Korth, H., B. J. Anderson, C. L. Johnson, R. M. Winslow, J. A. Slavin, M. E. Purucker, S. C. Solomon, and R. L. McNutt Jr. (2012), Characteristics of the plasma distribution in Mercury's equatorial magnetosphere derived from MESSENGER Magnetometer observations, *J. Geophys. Res.*, *117*, A00M07, doi:10.1029/2012JA018052.

Lammer, H., P. Wurz, M. R. Patel, R. Killen, C. Kolb, S. Massetti, S. Orsini, and A. Milillo (2003), The variability of Mercury's exosphere by particle and radiation induced surface release processes, *Icarus*, *166*, 238–247, doi:10.1016/j.icarus.2003.08.012.

Lavraud, B., et al. (2005), Cluster observes the high-altitude cusp region, *Surv. Geophys.*, *26*, 135–175, doi:10.1007/s10712-005-1875-3.

Leblanc, F., and R. E. Johnson (2003), Mercury's sodium exosphere, *Icarus*, *164*, 261–281, doi:10.1016/S0019-1035(03)00147-7.

Leblanc, F., and R. E. Johnson (2010), Mercury exosphere, I. Global circulation model of its sodium component, *Icarus*, *209*, 280–300, doi:10.1016/j.icarus.2010.04.020.

Lockwood, M., and M. F. Smith (1994), Low and middle altitude cusp particle signatures for general magnetopause reconnection rate variations. 1: Theory, *J. Geophys. Res.*, *99*, 8531–8553, doi:10.1029/93JA03399.

Lockwood, M., M. O. Chandler, J. L. Horwitz, J. H. Waite, T. E. Moore, and C. R. Chappell (1985), The cleft ion fountain, *J. Geophys. Res.*, *90*, 9736–9748, doi:10.1029/JA090iA10p09736.

Massetti, S., S. Orsini, A. Milillo, A. Mura, E. De Angelis, H. Lammer, and P. Wurz (2003), Mapping of the cusp plasma precipitation on the surface of Mercury, *Icarus*, *166*, 229–237, doi:10.1016/j.icarus.2003.08.005.

McClintock, W. E., and M. R. Lankton (2007), The Mercury Atmospheric and Surface Composition Spectrometer for the MESSENGER mission, *Space Sci. Rev.*, *131*, 481–521, doi:10.1007/s11214-007-9264-5.

McLain, J. L., A. L. Sprague, G. A. Grieves, D. Schriver, P. Travinicek, and T. M. Orlando (2011), Electron-stimulated desorption of silicates: A potential source for ions in Mercury's space environment, *J. Geophys. Res.*, *116*, E03007, doi:10.1029/2010JE003714.

Milillo, A., et al. (2005), Surface-exosphere-magnetosphere system of Mercury, *Space Sci. Rev.*, *117*, 397–443, doi:10.1007/s11214-005-3593-z.

Moebius, E., D. Hovestadt, B. Klecker, M. Scholer, and G. Gloeckler (1985), Direct observation of He^+ pick-up ions of interstellar origin in the solar wind, *Nature*, *318*, 426–429, doi:10.1038/318426a0.

Newell, P. T., and C.-I. Meng (1988), Hemispherical asymmetry in cusp precipitation near solstices, *J. Geophys. Res.*, *94*, 2643–2648, doi:10.1029/JA093iA04p02643.

Paschmann, G., G. Haerendel, N. Sckopke, H. Rosenbauer, and P. C. Hedgecock (1976), Plasma and magnetic field characteristics of the distant polar cusp near local noon: The entry layer, *J. Geophys. Res.*, *81*, 2883–2899, doi:10.1029/JA081i016p02883.

Raines, J. M., J. A. Slavin, T. H. Zurbuchen, G. Gloeckler, B. J. Anderson, D. N. Baker, H. Korth, S. M. Krimigis, and R. L. McNutt Jr. (2011), MESSENGER observations of the plasma environment near Mercury, *Planet. Space Sci.*, *59*, 2004–2015, doi:10.1016/j.pss.2011.02.004.

Raines, J. M., et al. (2013), Distribution and compositional variations of plasma ions in Mercury's space environment: The first three Mercury years of MESSENGER observations, *J. Geophys. Res. Space Physics*, *118*, 1604–1619, doi:10.1029/2012JA018073.

Retterer, J. M., T. Chang, and J. R. Jasperse (1983), Ion acceleration in the suprauroral region: A Monte Carlo model, *Geophys. Res. Lett.*, *10*, 583–586, doi:10.1029/GL010i007p00583.

Rosenbauer, H., H. Gruenwaldt, M. D. Montgomery, G. Paschmann, and N. Sckopke (1975), Heos 2 plasma observations in the distant polar magnetosphere: The plasma mantle, *J. Geophys. Res.*, *80*, 2723–2737, doi:10.1029/JA080i019p02723.

Roth, I., and M. K. Hudson (1985), Lower hybrid heating of ionospheric ions due to ion ring distributions in cusp, *J. Geophys. Res.*, *90*, 4191–4203, doi:10.1029/JA090iA05p04191.

Sarantos, M., J. A. Slavin, M. Benna, S. A. Boardsen, R. M. Killen, D. Schriver, and P. Trávníček (2009), Sodium-ion pickup observed above the magnetopause during MESSENGER's first Mercury flyby: Constraints on neutral exospheric models, *Geophys. Res. Lett.*, *36*, L04107, doi:10.1029/2008GL036747.

Shue, J. H., J. K. Chao, H. C. Fu, C. T. Russell, P. Song, K. K. Khurana, and H. J. Singer (1997), A new functional form to study the solar wind control of the magnetopause size and shape, *J. Geophys. Res.*, *102*, 9497–9511, doi:10.1029/97JA00196.

Slavin, J. A., et al. (2008), Mercury's magnetosphere after MESSENGER's first flyby, *Science*, *321*, 85–89, doi:10.1126/science.1159040.

Slavin, J. A., et al. (2010), MESSENGER observations of extreme loading and unloading of Mercury's magnetic tail, *Science*, *329*, 665–668, doi:10.1126/science.1188067.

Slavin, J. A., et al. (2012), MESSENGER observations of a flux-transfer-event shower at Mercury, *J. Geophys. Res.*, *117*, A00M06, doi:10.1029/2012JA017926.

Smith, M. F., and M. Lockwood (1996), Earth's magnetospheric cusps, *Rev. Geophys.*, *34*, 233–260, doi:10.1029/96RG00893.

Solomon, S. C., R. L. McNutt Jr., R. E. Gold, and D. L. Domingue (2007), MESSENGER mission overview, *Space Sci. Rev.*, *131*, 3–39, doi:10.1007/s11214-007-9247-6.

Sonnerup, B. U. Ö. (1974), Magnetopause reconnection rate, *J. Geophys. Res.*, *79*, 1546–1549, doi:10.1029/JA079i010p01546.

Sonnerup, B. U. Ö., G. Paschmann, I. Papmastorakis, N. Sckopke, G. Haerendel, S. J. Bame, J. R. Asbridge, J. T. Gosling, and C. T. Russell (1981), Evidence for magnetic field reconnection at the Earth's magnetopause, *J. Geophys. Res.*, *86*, 10,049–10,067, doi:10.1029/JA086iA12p10049.

Spreiter, J. R., A. L. Summers, and A. Y. Alksne (1966), Hydromagnetic flow around the magnetosphere, *Planet. Space Sci.*, *14*, 223–253, doi:10.1016/0032-0633(66)90124-3.

Sundberg, T., et al. (2012), MESSENGER observations of dipolarization events in Mercury's magnetotail, *J. Geophys. Res.*, *117*, A00M03, doi:10.1029/2012JA017756.

Vervack, R. J., Jr., W. E. McClintock, R. M. Killen, A. L. Sprague, B. J. Anderson, M. H. Burger, E. T. Bradley, N. Mouawad, S. C. Solomon, and N. R. Izenberg (2010), Mercury's complex exosphere: Results from MESSENGER's third flyby, *Science*, *329*, 672–675, doi:10.1126/science.1188572.

Winslow, R. M., C. L. Johnson, B. J. Anderson, H. Korth, J. A. Slavin, M. E. Purucker, and S. C. Solomon (2012), Observations of Mercury's northern cusp region with MESSENGER's Magnetometer, *Geophys. Res. Lett.*, *39*, L08112, doi:10.1029/2012GL051472.

Winslow, R. M., B. J. Anderson, C. L. Johnson, J. A. Slavin, H. Korth, M. E. Purucker, D. N. Baker, and S. C. Solomon (2013), Mercury's magnetopause and bow shock from MESSENGER Magnetometer observations, *J. Geophys. Res. Space Physics*, *118*, 2213–2227, doi:10.1002/jgra.50237.

Zurbuchen, T. H., G. Gloeckler, J. C. Cain, S. E. Lasley, and W. Shanks (1998), A low-weight plasma instrument to be used in the inner heliosphere, in *Conference on Missions to the Sun II*, Proc. Soc. Photo-Opt. Instrum. Eng. (SPIE), vol. 3442, edited by C. M. Korendyke, pp. 217–224, doi:10.1117/12.330260.

Zurbuchen, T. H., et al. (2011), MESSENGER observations of the spatial distribution of planetary ions near Mercury, *Science*, *333*, 1862–1865, doi:10.1126/science.1211302.